communications physics

ARTICLE

https://doi.org/10.1038/s42005-022-00876-5 OPEN

A three step recipe for designing auxetic materials on demand

Daniel Acuna [1,2], Francisco Gutiérrez[1,2], Rodrigo Silva[2,3], Humberto Palza[2,3], Alvaro S. Nunez[1,2,4] & Gustavo Düring [2,5]✉

Unlike regular elastic materials, when auxetic materials are compressed, they become thinner in the direction perpendicular to the applied force. Despite their outstanding mechanical properties, a systematic design of new and controlled auxetics remains underdeveloped. Here we establish a unified framework to describe bidimensional perfect auxetics with potential use in the design of new materials. Inspired by a natural connection between rotating rigid units and antiferromagnetic spin systems, we unveil the conditions for the emergence of a non-trivial floppy mode responsible for the auxetic behaviour. This model establishes three simple steps to design new auxetics. In particular, we constructed an exotic crystal, a Penrose quasi-crystal and the long-desired isotropic auxetic. The auxeticity of these designs is robust under small structural disturbances, as seen from experiments and numerical simulations. We expect that this work will allow the implementation of auxetic behaviour into advanced materials to enhance their functionalities, with a promising extension into 3D auxetics.

[1] Departamento de Física, Facultad de Ciencias Físicas y Matemáticas, Universidad de Chile, Santiago, Chile. [2] ANID - Millenium Nucleus of Soft Smart Mechanical Metamaterials, Santiago, Chile. [3] Departamento de Ingeniería Química, Biotecnología y Materiales, Facultad de Ciencias Físicas y Matemáticas, Universidad de Chile, Santiago, Chile. [4] CEDENNA, Avda. Ecuador 3493, Santiago, Chile. [5] Instituto de Física, Pontificia Universidad Católica de Chile, Casilla 306, Santiago, Chile. ✉email: gduring@uc.cl

The design of new materials with unusual mechanical properties and advanced functionalities has become a very active field of research in soft matter physics. These so-called mechanical metamaterials acquire their mysterious behaviour from the particular inner architecture and not from the properties of the constituent materials. In recent years, metamaterials have been engineered to display topological protection[1–6], programmable shapes[7–11], nonlinear response[2,10–14] and negative elastic constants[12,13,15–17] among others. Auxetic materials are probably the epitome of mechanical metamaterials, which were for the first time intentionally designed by Lakes in 1987[15]. An auxetic material, unlike common elastic materials, when compressed (expanded) in a given direction, compresses (expands) in the perpendicular direction. This unusual property is characterised by a negative Poisson's ratio ν, the ratio between the strain in one direction and the strain in its perpendicular direction.

A negative Poisson's ratio has been found in natural bioauxetics[18,19] and molecular auxetics[20,21]. Nowadays, with the onset of 3D printing, a wide range of auxetic materials are being developed[11,13,16,22–28], with interest in their enhanced mechanical properties, like increased energy absorption[29], enhanced indentation resistance[30], high fracture toughness[31], synclastic curvature in bending[32], and variable permeability[33], with applications in bio-medicine[34] and textiles[35] as some examples.

A variety of shapes and geometries have been identified as prototypical auxetics. The list ranges from re-entrant structures[36] to rotating units[37,38]. Chiral structures[39] and sliding bars systems[40–42] complete the list. Despite the extensive literature and enormous progress describing different types of auxetic materials no fundamental microscopic principles for a unified description exist. The distinction between types of auxetics relies mainly on empirical observation rather than in fundamental principles, and no general prescription exists to build them. In this article, we present a unified framework for the description of bi-dimensional perfect auxetics. In this limit the bulk modulus vanishes while the shear modulus remains finite implying a perfect auxetic behaviour, i.e. with a Poisson's ratio $\nu = -1$ over a finite strain range[42,43]. Understanding and controlling the perfect auxetic limit allows us to rationally design realistic auxetics with a tailor-made geometric structure for which the Poisson's ratio remains negative. The precise value of the Poisson's ratio depends on the proximity to the ideal design and the energy interaction between the material constituents.

To our knowledge rotating unit models and sliding bars systems are the only ones that have displayed a perfect auxetic behaviour in a finite strain range. Both materials are quite related[41]. Rotating unit systems[16,23,34,37,38,44–46] can be considered as a material made of elastic units connected to their neighbours in such a way that the energy cost of deforming the bulk of each unit is much higher than that of deforming the bond between neighbours. Generically one can think of a structure made out of polygons connected through their vertices, as the ones in Fig. 1a. Under external loads the stresses focalise on the vertices leaving the bulk of the polygons almost undeformed. The auxetic behaviour arises because neighbour polygons tend to rotate in opposite directions along a particular low energy mode. This mode is reminiscent of a non-trivial floppy mode, or mechanism, that exists in the limit case with zero bending energy (i.e. the polygons are connected through ideal hinges) which leads to a perfect auxetic behaviour[45]. If polygons are considered as rigid structures, an extended version of the Maxwell's degrees of freedom counting argument[47] shows that auxetic polygon networks of rotating unit systems are isostatic or overconstrained (Supplementary Note 1). Therefore, the existence of an "auxetic" floppy mode must be related to a very precise geometrical construction which also implies the appearance of a non-trivial self stress state mode following the rank theorem[48]. No general conditions for the emergence of this floppy mode exist, except for certain limited sets of periodic lattices[49,50]. Other auxetics have different origins, for instance, reentrant materials have typically an under-constrained internal structure stabilised by bending or angular forces[43]. Therefore, the shear and the bulk modulus vanishes in the zero bending limit, excluding a priori the existence of a perfect auxetic behaviour.

To understand the auxetic behaviour of rotating units systems we restrict our study to their perfect auxetic limit. This can be easily achieved considering a minimal model of rigid polygons connected by springs of zero natural length[46]. The springs act as ideal hinges as long as they are not compressed or stretched. Since rigid polygons can only rotate, any floppy mode requires that all the neighbours of each polygon have the same rotation rate (as a function of strain). If the neighbours of a given polygon are also neighbours between them the system will then jam. A similar behaviour is observed for antiferromagnetic spin systems, if the neighbours of a spin are also neighbours between them the antiferromagnetic phase will be frustrated. A pure antiferromagnetic phase is known to be achieved only for bipartite networks. This similarity sets the key ingredient for rotating units auxetic theory, which requires the system to be bipartite as well, as can be easily check for all previous rotating units auxetics. As we will discuss later, the connection with spin systems can be pushed further by looking at the potential energy of our model which can be mapped to an anisotopic antiferromagnetic spin systems. Exchanging temperature with strain a Ginzburg-Landau energy can be constructed leading to a general descriptions of domain walls in auxetic materials, a phenomena recently observed in refs. [23,46]. Although bipartite polygon networks are a necessary condition, and most of them show some level of auxetic response, additional conditions are necessary to obtain a perfect auxetic behaviour.

Our theory not only unifies a large class of existing auxetics, encompassing previous auxetic rigid units systems, but also allows to create a large variety of them, with new and diverse geometries, including the somewhat elusive isotropic auxetic material[43,51]. In Fig. 1 one can see three different examples of elastic structures based on perfect auxetic designs; a new type of auxetic crystals, a quasicrystal and an isotropic (disordered) structure. These structures where 3D printed on elastic resin, their mechanical response was measured and compared against finite element simulations performed on the software Ansys (Supplementary Note 3). After a finite initial load, they display a clear auxetic behaviour with a Poisson's ratio reaching values between -0.62 and -0.14, as shown in Fig. 1b. The precise value of the Poisson's ratio depends mainly on how close the design is to the ideal scenario, i.e. zero bending to stretching energy ratio. This behaviour can be easily controlled by changing the thickness of the bonds between polygons[16]. An example of this is shown in Fig. 1c, where two Penrose auxetics with different bond thickness are compared, the design with thinner bonds and therefore lower bending to stretching energy ratio shows a smaller Poisson's ratio closer to the ideal value. By design, by decreasing the bonds thickness the Poisson's ratio must decrease, eventually reaching the ideal limit $\nu = -1$ when the bonds behave as ideal hinges.

Here we show a framework to build and analize bidimensional perfect auxetics composed of rigid units. With it we uncover the origin of the auxetic floppy mode. Furthermore, crystals, quasicrystals and amorphous auxetics solids can be designed within our theory spanning all the general kinds of microscopic structure of solids. Thus, if a particular microscopic structure, such as a crystalline symmetry, is required for a material to perform a specific functionality, our theory provides a recipe to add an

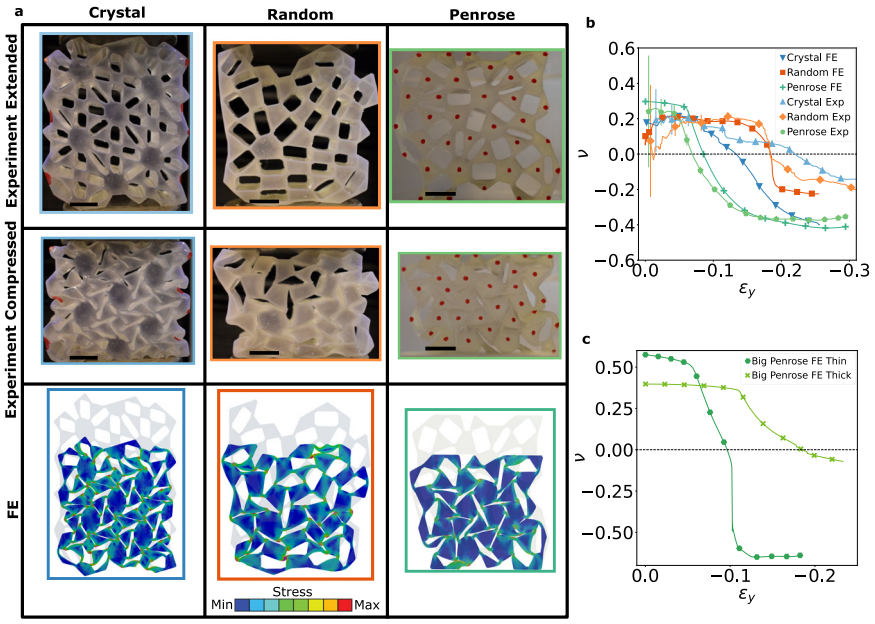

Fig. 1 Auxetic behaviour on demand. a Shows the uniaxial compression test of three auxetic designs, each of them generated with our proposed algorithm. More on Supplementary Movie 1 and 2. Scale bars 1 cm. The colormap on the finite element simulations shows the sections of minimum and maximum stress in the elastic material. Clearly the stress is focused on the joints between polygons. **b** The Poisson's ratio of each configuration as a function of the strain. "Exp" and "FE" refer to experimental and finite element simulations results respectively. The experimental error bars show the standard deviation from measuring each polygon's position. **c** Comparison between two bigger Penrose structures with thin and thick bonds, showing the capabilities of tuning the Poisson's ratio as a function of the bending energy. These bigger structures can be found on Supplementary Note 3. More information on the experimental and finite element simulations set-ups on Methods: "Experimental Setup" and "Finite Element Simulations" respectively.

auxetic response to the material. The consequences and applications of this feature are multiple. From the possible development of new compliant mechanisms, shape morphing materials, smart surfaces or actuators, crucial elements in the design of novel soft robots[52–54]. To a generalisation of the theory into perfect 3D auxetics.

Results and discussion

A simple model for perfect auxetics. We are interested in the behaviour of perfect auxetics, to build them we use the minimal bi-dimensional model for rotating units auxetics, consisting of a series of polygons connected by springs of zero natural length[46]. Each rigid unit has three degrees of freedom, two translational $\vec{x}_i = (x_i, y_i)$ and one rotational θ_i, not necessarily measured from the centroid of each polygon. This model allow to determine the emergence of the auxetic floppy mode and also introduces elasticity into our materials to study non-ideal scenarios. The recipe for building a perfect auxetic requires three ingredients.

- The network must be bipartite.
  This allows the units to counter rotate respect to each other, like cogs in a machine. The units arranged in a bipartite network can be separated in two sets A and B, i.e. each connected to the other but not to itself, see Fig. 2a.
- Initially and at rest, every pair of neighbouring polygons position's ($\vec{x}_i$, $\vec{x}_j$) and the vertex between them have to be collinear.
  This initial setting, matches a maximum extension configuration. Furthermore, it establishes a relationship between the internal angles of every pair of neighbouring polygons $|\alpha_{ij} + \beta_{ji}| = \pi$, see Fig. 2b.
- The ratio between the distance of a polygon to one of its vertex and the distance of his neighbour to the same vertex must be a constant in the network.
- The ratio of the size of neighbouring polygons $C = b_{ji}/a_{ij}$ must be a constant through the network, as seen in Fig. 2c.

Applying all these rules, we arrive to an auxetic polygon network which is ready to be printed as shown in Fig. 2d, e.

Each vertex of a rigid unit is characterised by a vector $\vec{a}_{ij} = a_{ij}(\cos(\theta_i + \alpha_{ij}), \sin(\theta_i + \alpha_{ij}))$ or $\vec{b}_{ji} = b_{ji}(\cos(-\theta_j - \beta_{ji}), \sin(-\theta_j - \beta_{ji}))$, corresponding to sets A or B respectively. The index i will be used for polygons in the set A and the index j for polygons in the set B. Vectors $\vec{a}_{ij}$ ($\vec{b}_{ji}$) point from the position $\vec{x}$ of the polygon $i(j)$ into the vertex connecting with polygon $j(i)$, as seen in Fig. 2f.

Creating a polygon network that fulfils these rules is quite simple. Starting from a planar bipartite graph one can always build a perfect auxetic. To understand the origin of this behaviour we turn to the energy of the polygon network

$$V = \frac{k}{2}\sum_{<ij>}\left((\vec{x}_i + \vec{a}_{ij}) - (\vec{x}_j + \vec{b}_{ji})\right)^2, \qquad (1)$$

where the sum is over all the pairs of interacting neighbours and all springs have an equal elastic coefficient k.

We shall consider the energy change under an isotropic compression, which is equivalent to increasing the size of all polygons while keeping the distance between polygons constant. From the second requirement, as the neighbouring polygons are initially collinear with their vertex, the constant distance between polygons is $\vec{x}_i - \vec{x}_j = -(a_{ij} + b_{ji})\begin{pmatrix}\cos(\alpha_{ij})\\ \sin(\alpha_{ij})\end{pmatrix}$. Increasing the size of the polygons is achieved by rescaling with λ the vectors characterising the vertices, such that $\vec{a}_{ij} \to \lambda \vec{a}_{ij}$ and

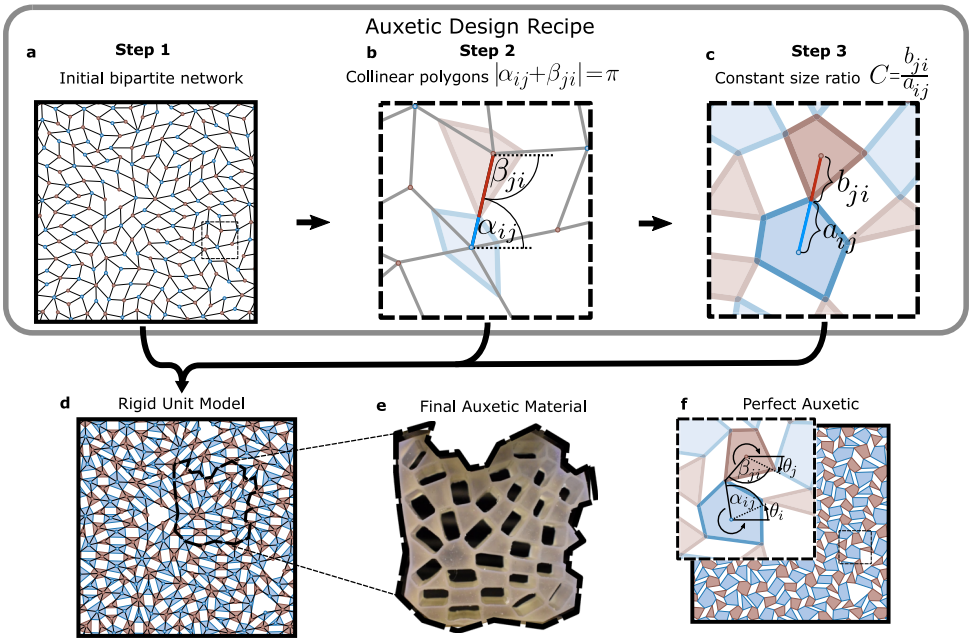

Fig. 2 The 3 steps recipe. a Step 1, we start with a bipartite network, the blue and red colours stand for the A and B sets respectively. We showcase a random bipartite network to demonstrate the versatility of this recipe. **b** Step 2, every node of the graph becomes the position of each polygon and we place each polygon's vertex on top of each corresponding segment of the network. At rest the polygon's position is collinear with its neighbour's position and the vertex between them. **c** Step 3, each polygon vertex is positioned such that the ratio $C = b_{ji}/a_{ij}$ remains constant along the network. a_{ij} is the distance from the node to each vertex in the A set polygons, b_{ji} is the analogue for the B set. **d** The resulting polygon network after performing the 3 steps. **e** A section of the final random auxetic design printed in 3D. As every section of the model is inherently a perfect auxetic, the printed material keeps being auxetic. **f** A compression shows that the polygon network is a perfect auxetic. In the zoom in we see how each polygon counter rotates with respect to its neighbours. θ_i and θ_j show the rotation of the A and B set respectively.

$\vec{b}_{ji} \to \lambda \vec{b}_{ji}$. Then we can expand and rearrange Eq. (1) as

$$V = V_0 + \sum_{<ij>} J_{ij}\cos(\theta_i + \theta_j) - H^A_{ij}\cos(\theta_i) - H^B_{ji}\cos(\theta_j). \quad (2)$$

In this equation $V_0 = \frac{k}{2}\sum_{<ij>}(a_{ij}+b_{ji})^2 + \lambda^2(a_{ij}^2 + b_{ji}^2)$, $J_{ij} = k\lambda^2 a_{ij}b_{ji}$, $H^A_{ij} = k\lambda(a_{ij}+b_{ji})a_{ij}$ and $H^B_{ji} = k\lambda(b_{ji}+a_{ij})b_{ji}$.

Using the third requirement, setting $C = b_{ji}/a_{ij}$ as a constant, two solutions can be found. The first one is the trivial solution $\theta_i = \theta_j = 0$ which is a minimum for $0 < \lambda \le 1$. The second one is found when all the polygons of each set rotate at the same rate $\theta_i = \theta^0_A$ and $\theta_j = \theta^0_B$, where

$$\cos(\theta^0_A) = \frac{1 + C + \lambda^2(1-C)}{2\lambda}, \quad (3)$$

and

$$\cos(\theta^0_B) = \frac{1 + C - \lambda^2(1-C)}{2\lambda C}. \quad (4)$$

These are a minimum in the range $1<\lambda<\left|\frac{1+C}{1-C}\right|$ only if both θ^0_A and θ^0_B have the same sign, i.e. polygons counter rotate respect to each other. Evaluating the potential energy in this minimum we find that $V(\theta_i = \theta^0_A, \theta_j = \theta^0_B) = 0$ (Supplementary Note 5), thus this solution describes a zero energy mode of the system. This floppy mode corresponds to a system with zero bulk modulus, meaning that the material expands and contracts equally in all directions, for a direct calculation of the bulk modulus see Supplementary Note 6. As the Poisson's ratio is defined as $\nu = -\frac{d\epsilon_x}{d\epsilon_y}$, with ϵ being the strain in each direction, and as λ compresses the system equally in all directions, then $\epsilon_x = \epsilon_y$ and $\nu = -1$.

For anisotropic materials, the Poisson's ratio could take values <-1. Hence the perfect auxetic definition does not always define the material with the lowest Poisson's ratio, but guarantees an equal auxetic response independent of the direction of external compression, representing the most symmetric case for anisotropic materials. This behaviour can be easily understood when a single floppy mode exists in these materials. Their Poisson's ratio in one direction must be the inverse in the perpendicular direction. Thus, if they have a Poisson's ratio ranging from 0 to -1, in the opposite direction it will range between $-\infty$ to -1 as seen in Supplementary Movie 4. This feature is quite interesting in the fields of strain amplification[55]. In Section: "Floppy modes on bipartite polygon networks" we will see a particular case of structures with a single floppy mode but non -1 Poisson's ratio.

Random perfect auxetics. Recently, several isotropic auxetics materials with a Poisson's ratio close to -1 in an infinitesimal strain range have been proposed[43,51]. However, none of them display a perfect auxetic behaviour. The theory presented previously is not restricted to lattices. It can be applied straightforwardly to disordered networks, which allow us to the best of our knowledge to build the first isotropic perfect auxetic materials. The only complication resides in building a planar bipartite disordered network. We achieved this by two different methods, a pruning algorithm, and a graph transformation, both applied on an isotropic amorphous contact network[14,56] (Methods: "Building Random Bipartite Planar Graphs"). Once we have our bipartite network, we only need to place polygons at each node of the graph, taking care that each vertex of the polygon is placed over a segment of the graph, dividing it in a C: 1 ratio, see Fig. 2.

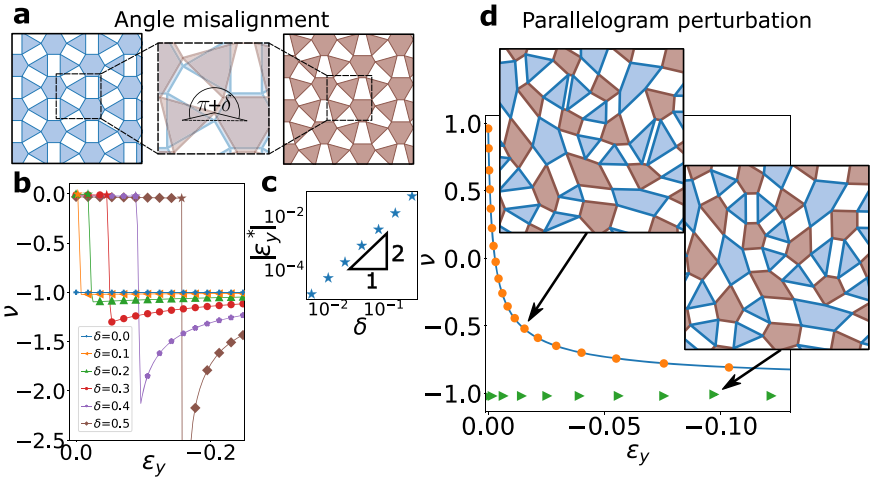

Fig. 3 Breaking the rules. Two interesting examples that break the rules to build a perfect auxetic. **a** Misaligning pairs of polygons by an angle δ, leaves them no longer collinear between them and their vertex. Notice that this perturbation turns the previously parallelogram holes into trapezoids. This effectively jams the system, delaying its auxetic response as seen in the Poisson's ratio in **b** (Supplementary Movie 3). Moreover, in **c** we see how the transition to the auxetic behaviour happens at a strain ϵ_y^*, which scales as δ^2. **d** Perturbating the geometry of a perfect auxetic (green triangles) while preserving the parallelogram property of the holes, results in the preservation of the non-trivial floppy mode in the system, while changing it's Poisson's ratio (orange circles). The Poisson's ratio of the perturbed system fits well with that of a rectangular auxetic (blue line)[23,37], see Supplementary Note 7 and Supplementary Movie 4. For more information about the measurements, see Supplementary Note 2.

Beyond perfect auxetics. The bipartite condition seems to be fundamental to have an auxetic material composed of rotating units. Introducing defects on the network will frustrate the rotation of the units affecting the auxetic behaviour. We consider the effect of breaking other conditions, for example by modifying the angle that connects two polygons, thus making $|\alpha_{ij} + \beta_{ji}| = \pi + \delta_{ij}$. For the sake of simplicity we used a periodic polygon network and a fixed δ that will change sign from one link to the next, see Fig. 3a. By perturbing the polygon network the floppy mode is destroyed and the polygon network jams. During compression, this deformation initially stabilizes the unrotated state, creating two distinct states for the system as seen in Fig. 3b. At small strains, it remains in a stable unrotated state, with a near zero Poisson's ratio. At higher strains the unrotated state is unstable, thus the system goes into an auxetic rotated state with a sudden drop in the Poisson's ratio. As the perturbation angle is increased, this change of state happens at a bigger characteristic strain ϵ_y^*. In Fig. 3c we present this characteristic strain as a function of the perturbation angle, showing how it scales as δ^2.

Although the latter behaviour seem to be generic under small perturbations of the perfect auxetic network it is not always the case. It is known that rectangular networks[23], which are not perfect auxetics, preserve a floppy mode and the Poisson's ratio moves continuously from positive to negative values. To understand the condition for the existence of this floppy mode we need a more general description on polygon bipartite networks.

Floppy modes on bipartite polygon networks. Bipartite graphs have only even sided cycles, these are closed paths that start and end at the same node. The simplest of cycles are the faces of the graph, which are the regions bounded by edges. When transforming a bipartite graph into a polygon network, even cycles are reflected at the geometry of empty spaces between the polygons which are also enclosed by the same number of sides. We will refer to this empty spaces as holes, and to the vertex between polygons as hinges. Notice that no odd-sided holes can exist in bipartite systems. In the case of our perfect auxetic materials, one can use the Varignon's quadrilateral theorem[57] and Thales theorem to show that the constant ratio $C = b_{ji}/a_{ij}$ directly implies that all 4 sided holes will be parallelograms.

For a system to be deformed while at zero energy, it needs the opposite angles at each hinge to have an opposite deformation rate. This condition is in general extremely difficult to fulfil, except if all 4 sided holes are parallelograms. They have the special property that when deformed, all of their inner angles share the same deformation rate, except for the sign. All 4 sided holes in perfect auxetics are parallelograms, this allows every inner angle in each hole to be linearly related to the deformation, fulfilling the restriction at each hinge. This mechanism suggests that any bipartite polygon network with only parallelogram holes will have a non-trivial floppy mode. However, it will not necessarily behave like a perfect auxetic. This inner angles analysis is similar to the "vertex model"[58].

When geometrically perturbing the polygons of a perfect auxetic with only four-sided holes, while preserving their parallelogram shape, the floppy mode persists. The simplest example is the rectangular network previously studied in[23,37]. Similar results are observed in a more general case where four-sided holes remain parallelograms after a perturbation of an isotropic perfect auxetic. A singular behaviour is observed as soon as a perturbation is added, showing a Poisson's ratio equal to 1 under an infinitesimal strain (see Fig. 3d). For larger strains, Poisson's ratio approaches a higher value as perturbation is increased. Moreover, we observe that these random perturbed materials and rectangular auxetics[23,37] have a similar behaviour for the Poisson's ratio, as seen in the fit in Fig. 3d. If compression is applied in the opposite direction the Poisson's ratio will have the inverse value, as the system has a single floppy mode. More information on this similarity and the perturbation, on Supplementary Note 7.

Domain Walls. Strikingly, not only the rotation of the polygons resembles that of an antiferromagnetic spin system, Fig. 4a, but also does the structure of equation (2). Where θ represents the spin direction, J_{ij} is a symmetric coupling and $H_i = \sum_n H_{in}$, where n sums over neighbours, is analogous to a magnetic field as a

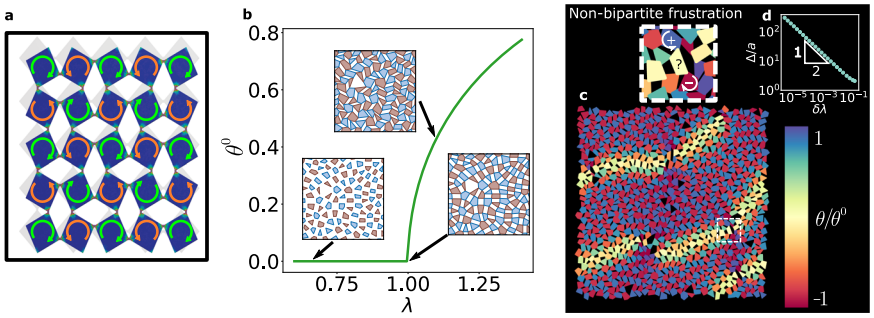

Fig. 4 Antiferromagnet spin analogy. a Finite element simulation of a square units auxetic. The auxetic basic mechanism lies in the coordination and synchronisation of the buckling instability at each of the weak links that provide the structure its stability. The effective collective pattern that emerges is analogue to an antiferromagnetic arrangement. Each of the two interconnected lattices that fit the bipartite system rotate in opposite directions, as indicated by the green and orange arrows. **b** The rotation angle θ^0 as a function of the compression λ, for $C = 1$. Analogous to an antiferromagnetic system, the material goes through a phase transition from a stretched state, to a compressed rotated state. With its critical point located at at $\lambda = 1$. **c** By breaking the bipartivity the auxetic will frustrate, creating local defects that don't rotate as predicted. Here we showcase a non-bipartite random polygon network, when compressed a system spanning defect appears (yellow), reminiscent of a domain wall. The colour represents the rotation of each polygon, red being clockwise and blue counter clock wise, yellow shows the frustrated polygons. To create this defect, periodic boundary conditions where applied to an initially bipartite network, this boundary condition created a non-local odd cycle which destroyed the bipartivity. **d** The domain wall length Δ, normalised by the polygon size a, plotted against the isotropic expansion parameter $\delta\lambda$, it's evident that $\Delta \sim \delta\lambda^{-1/2}$, more on Supplementary Note 4.

function of space. Moreover, from Fig. 4b we can see that the system has a critical point $\lambda = 1$ where the polygon's angle goes from zero to a rotated state. From Eqs. (3) and (4) we can see that similarly to a spin system, close to the critical point the angle grows as the root of an external parameter $\theta \sim \sqrt{\frac{2}{C}}\delta\lambda^{1/2}$, here $\delta\lambda = \lambda - 1$. Considering these factors and neglecting the polygon displacements we can build an energy functional for this model, with a normalised polygon angle $\theta(x)$ as an order parameter,

$$H = \int dx \left(\frac{-t_0 \delta\lambda}{2} \theta(x)^2 + u\theta(x)^4 + \frac{K}{2} (\nabla\theta(x))^2 \right). \qquad (5)$$

Where t_0, u and K are positive constants, and $u = \frac{C}{8} t_0$. This model predicts the appearance of domain walls like the one in Fig. 4c, with a characteristic length $\Delta \sim \delta\lambda^{-1/2}$, which perfectly agrees with the numerical simulations of periodic perfect auxetics, Fig. 4d. The exact calculations and simulations are shown in Supplementary Note 4.

Conclusions

We have presented a simple model that builds the necessary framework to create, design, and characterise rotating unit auxetics. Such framework is built upon a simple analogy between the rotating unit auxetics and an anisotropic XY antiferromagnetic system. As shown in Fig. 1, we have applied those ideas to generate novel auxetic structures in the form of a crystal, a quasicrystal, and a random lattice. Each design can be represented, within our theory, by a minimal model, based upon polygons and springs that captures its essential collective response to external loads. These models can be simulated straightforwardly to test materials properties while ignoring bending forces. However, if needed, bending can easily be added to the model. As we have seen, this model correctly describes the behaviour of all rotating units systems and could be used to predict new behaviours. In particular, we have generalised the behaviour of auxetic domain walls, which are natural textures that these systems have because of the analogy with magnetic systems. More phenomena related to this analogy remain to be seen and encourage further investigation. As a major tangible result, our work leads us to establish the ground rules to create never seen before isotropic perfect auxetics. This model still lacks dynamic and vibrational analysis that, hopefully, will shed light on the general topological properties of these materials. Furthermore, this theory has the potential to be expanded into 3D polyhedral materials, as it is mainly written in a vectorial form, we are excited to see where this takes us.

Methods

Experimental setup. Network Design: For the simulations and experiments in Fig. 1, we used three bipartite networks which were created using the methods described in Methods section: "Building Random Bipartite Planar Graphs". For the exotic crystal we modified a tetrakis tiling by skewing it and applying the bipartite transformation; for the quasi-crystal we used a Penrose tiling which was cut in a suitable square shape; lastly the random network was created using the pruning method. All the materials were built with the same ratio between average polygon size and bond thickness, such that they exhibit a similar behaviour.

Materials: a commercial elastic resin (code name Elastic 50*A*) from Formlabs was used for the direct 3D printing of the auxetic structures. From the several available resins, Elastic 50*A* presented the elasticity needed for the tests further allowing a printed structure with the proper resolution. The mechanical characteristics of the material are 160% of elongation at failure, 19.1 kNm^{-1} of tear strength, 3.23 MPa of ultimate tensile strength and 50 A of shore hardness[59].

3D Printing: a Form 2 3D printer from Formlabs was used to print directly the auxetic structures avoiding the need to print a negative mould. The model file was loaded in the Preform software of the 3D printer for size adjustments and the addition of the corresponding supports. We tested different sizes until the direct printing allowed a structure with the proper elasticity and resolution avoiding defects and imperfections. The structures were defined having at least 40 rigid units. The final dimensions of the structures (height × width × thickness) were $56 \times 57 \times 20$ mm for the random structure and $68 \times 55 \times 20$ mm for the exotic crystal, and $58 \times 58 \times 20$ mm for the Penrose structure, they were printed with 100 µm of layer thickness resolution.

The compression tests were carried out in a Jinan mechanical tester model WDW-S5 using a 5-kN cell and a velocity of 0.83 mms^{-1}. The compression was applied until a 30% of deformation approximately. A professional camera Nikon D5300 was used to record the sample during compression and expansion. From these images we tracked the position of each rigid unit, which we used to measure the Poisson's ratio.

Finite element simulations. For our static finite elements simulations, we used the commercial software ANSYS[60] and a Neo-Hookean energy density as a material model, with an initial shear modulus, $G = 0.15MPa$, and Poisson's ratio $\nu = 0.5$, and in-plane strain conditions with hybrid quadratic triangular elements (ANSYS type PLANE183[61]). We carried out a mesh optimisation to ensure that bonds, where most of the strain and stress is localised, are meshed with at least three

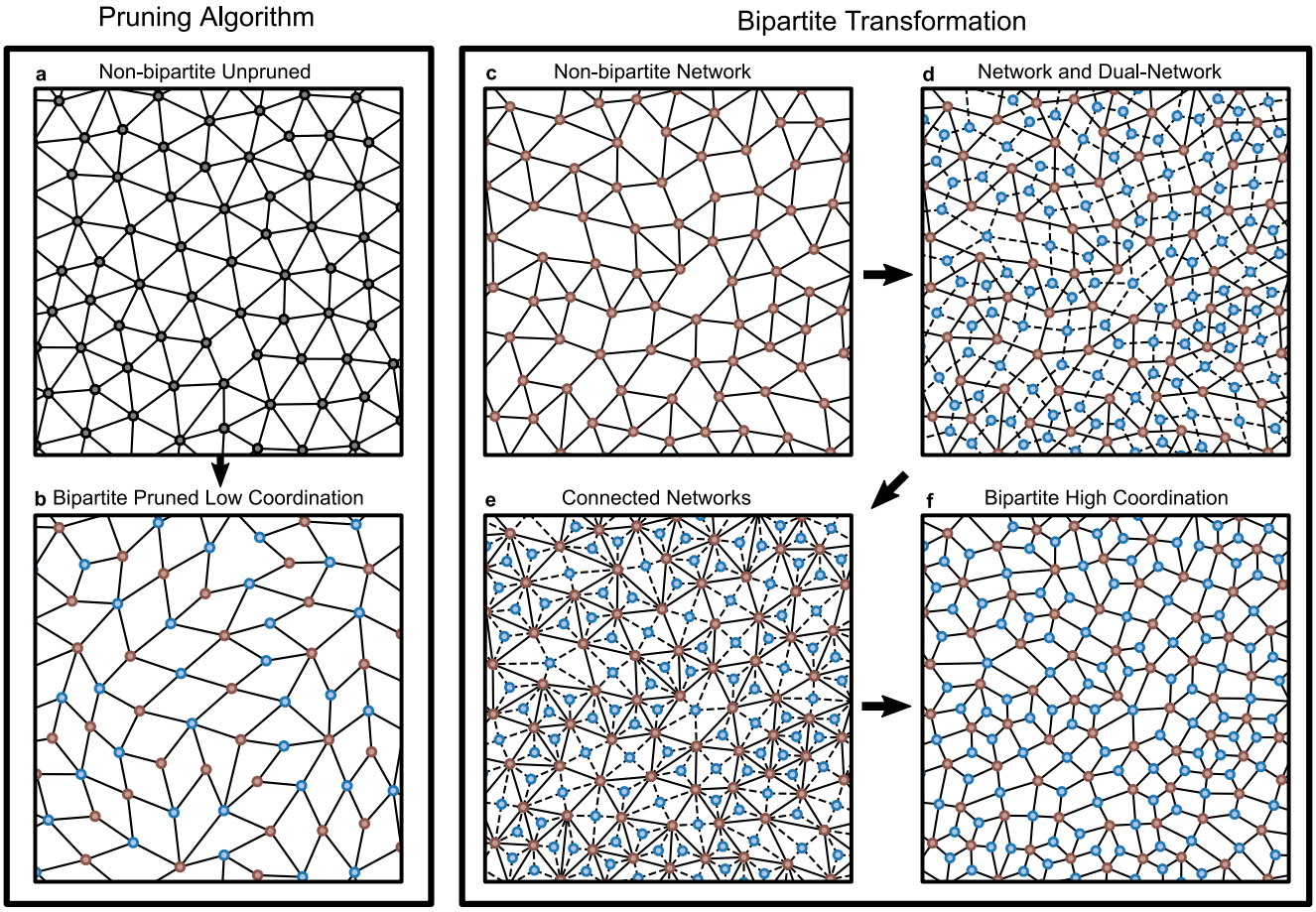

Fig. 5 Two methods to build random bipartite planar graphs. Both start from an isotropic contact amorphous network[14,56]. **a** Starting network with a high coordination $z = 6$. **b** Pruned version of the previous network, the bonds between pairs of odd cycles have been removed, adding them together into even cycles. The result is a bipartite planar graph. **c** Starting random planar contact network, in this case the coordination is $z = 5$. **d** We compute the dual graph of the network (blue nodes and dashed lines), place each node of the dual graph inside its corresponding cycle. **e** Then disconnect each node of the dual graph (blue to blue nodes), and reconnect them to the nodes corresponding to the vertices of its cycle in the original graph (red and blue nodes connected by dashed lines). **f** Lastly remove the connections of the original graph (red to red nodes) and keep the connections between the dual graph and the original graph. As both initial graphs are independent sets that don't connect to themselves, the result is a random planar bipartite graph.

elements. This way, the material has 10^5 elements approximately. To compress the material uniaxially, we applied a vertical displacement of the top row of polygons, and fixed the position of the bottom row of polygons. We imposed a free boundary condition in the horizontal direction and we imposed a no-penetration condition, therefore the material can contact itself.

Building random bipartite planar graphs. One of the main problems in creating a random perfect auxetic material is the construction of a random bipartite planar graph, from which we can construct the polygon network. The graph must be bipartite so that the polygons can counter rotate with respect to each other, and it must be planar so that we can build the polygon network without overlapping them.

We propose two methods to create these graphs. The first is a heuristic pruning algorithm, which takes advantage of the property that a graph with only even cycles will be bipartite. The second is a general transformation that can quickly create bipartite graphs by combining a graph with its dual graph.

Pruning algorithm. A bipartite graph has only even cycles, where a cycle is the shortest path between a node and itself. We call a cycle even or odd depending on the number of bonds in its path. Here we prune a graph in such a way that all the cycles of the resulting graph are even, transforming the graph into a bipartite graph.

If we have two neighbouring cycles that share a bond, and we prune this bond, we will end up with a single cycle. We can think of this operation as an addition of cycles. Where if the starting cycles are both even or odd, the resulting cycle will be even. And if one cycle is even and the other is odd, the resulting cycle is odd. We can extrapolate this property to a pair of separate odd cycles with only even cycles between them. If we remove a line of bonds between the odd cycles, we will end up with a single even cycle. Then, if we prune the bonds between all pairs of odd cycles, we will end up with a bipartite graph with only even cycles.

The pruning algorithm we implemented follows some simple steps, we start with a random planar graph with an even number of odd cycles, ideally with a high coordination number, e.g. $z = 6$. Next, we place a marker at an odd cycle and use a breadth-first search algorithm on the dual graph, to find the path to its closest odd cycle. We remove the bonds in this path, transforming both odd cycles into a single even cycle. Finally we move the marker to another odd cycle and repeat the procedure until all cycles are even. An example of the initial and final graphs is in Fig. 5. While removing bonds we prefer paths that leave each node with at least three bonds, to give the system more stability and to avoid generating big holes. If a node is left with less than two links, we eliminate the node.

This algorithm works well on small graphs, but on bigger ones it may eliminate a huge amount of bonds leaving big holes. To avoid this problem a more sophisticated path optimisation algorithm is needed, where the paths between all pairs of odd cycles are calculated beforehand, minimising the distance of each path and making sure they avoid each other. Once all of the paths are computed, the bond elimination process can be performed, minimising the size of the holes. Furthermore, this algorithm does not necessarily work for graphs with periodic boundary conditions. As having only even sided cycles guarantees bipartivity if the graph has free boundary conditions, but it does not if the graph has periodic boundary conditions.

Bipartite transformation. A bipartite graph is made out of two independent sets, each one connected to the other but note to itself. Here we connect two independent sets, a graph and its dual graph, transforming both into a single planar bipartite graph.

Given a graph, we first determine its dual graph. Then we connect each node of the graph with each neighbouring node in the dual graph, by neighbour node we mean the node in the dual graph that represents a face in contact with the node in the original graph. At last, we eliminate all the starting bonds of the graph and its dual graph, leaving only the new bonds connecting both graphs. The resulting graph will be bipartite, and if the original graph was planar, the resulting graph will be planar too. To further understand this procedure, see Fig. 5.

This transformation can be performed on any kind of graph and several times in a row creating a graph with more nodes each time. We can reverse the transformation, though we may not know if we obtained the graph or its dual graph when performing the inverse transformation, unless we keep track of at least one node from the starting graph.

Data availability

The data that support the plots within this paper and other findings of this study are available from the corresponding author upon request.

Received: 23 July 2021; Accepted: 17 February 2022;
Published online: 10 May 2022

References

1. Huber, S. D. Topological mechanics. *Nat. Phys.* **12**, 621–623 (2016).
2. Coulais, C., Sounas, D. & Alù, A. Static non-reciprocity in mechanical metamaterials. *Nature* **542**, 461–464 (2017).
3. Kane, C. & Lubensky, T. Topological boundary modes in isostatic lattices. *Nat. Phys.* **10**, 39–45 (2014).
4. Chen, B. G., Upadhyaya, N. & Vitelli, V. Nonlinear conduction via solitons in a topological mechanical insulator. *Proc. Natl Acad. Sci. USA* **111**, 13004–13009 (2014).
5. Rocklin, D. Z., Zhou, S., Sun, K. & Mao, X. Transformable topological mechanical metamaterials. *Nat. Commun.* **8**, 1–9 (2017).
6. Souslov, A., Van Zuiden, B. C., Bartolo, D. & Vitelli, V. Topological sound in active-liquid metamaterials. *Nat. Phys.* **13**, 1091–1094 (2017).
7. Florijn, B., Coulais, C. & van Hecke, M. Programmable mechanical metamaterials. *Phys. Rev. Lett.* **113**, 175503 (2014).
8. Coulais, C., Teomy, E., De Reus, K., Shokef, Y. & Van Hecke, M. Combinatorial design of textured mechanical metamaterials. *Nature* **535**, 529–532 (2016).
9. Overvelde, J. T., Weaver, J. C., Hoberman, C. & Bertoldi, K. Rational design of reconfigurable prismatic architected materials. *Nature* **541**, 347–352 (2017).
10. Mullin, T., Deschanel, S., Bertoldi, K. & Boyce, M. C. Pattern transformation triggered by deformation. *Phys. Rev. Lett.* **99**, 084301 (2007).
11. Shim, J., Perdigou, C., Chen, E. R., Bertoldi, K. & Reis, P. M. Buckling-induced encapsulation of structured elastic shells under pressure. *Proc. Natl Acad. Sci. USA* **109**, 5978–5983 (2012).
12. Nicolaou, Z. G. & Motter, A. E. Mechanical metamaterials with negative compressibility transitions. *Nat. Mater.* **11**, 608–613 (2012).
13. Coulais, C., Overvelde, J. T. B., Lubbers, L. A., Bertoldi, K. & van Hecke, M. Discontinuous buckling of wide beams and metabeams. *Phys. Rev. Lett.* **115**, 044301 (2015).
14. Wyart, M., Liang, H., Kabla, A. & Mahadevan, L. Elasticity of floppy and stiff random networks. *Phys. Rev. Lett.* **101**, 215501 (2008).
15. LAKES, R. Foam structures with a negative poisson's ratio. *Science* **235**, 1038–1040 (1987).
16. Bertoldi, K., Reis, P. M., Willshaw, S. & Mullin, T. Negative poisson's ratio behavior induced by an elastic instability. *Adv. Mater.* **22**, 361–366 (2010).
17. Lakes, R. S., Lee, T., Bersie, A. & Wang, Y. Extreme damping in composite materials with negative-stiffness inclusions. *Nature* **410**, 565–567 (2001).
18. Williams, J. & Lewis, J. Properties and an anisotropic model of cancellous bone from the proximal tibial epiphysis. *J. Biomech. Eng.* **104**, 50–56 (1982).
19. Pagliara, S. et al. Auxetic nuclei in embryonic stem cells exiting pluripotency. *Nat. Mater.* **13**, 638–644 (2014).
20. Baughman, R. H., Shacklette, J. M., Zakhidov, A. A. & Stafström, S. Negative poisson's ratios as a common feature of cubic metals. *Nature* **392**, 362–365 (1998).
21. Grima, J. N., Gatt, R., Alderson, A. & Evans, K. E. On the origin of auxetic behaviour in the silicate α-cristobalite. *J. Mater. Chem.* **15**, 4003–4005 (2005).
22. Coulais, C., Kettenis, C. & van Hecke, M. A characteristic length scale causes anomalous size effects and boundary programmability in mechanical metamaterials. *Nat. Phys.* **14**, 40–44 (2018).
23. Florijn, B., Coulais, C. & van Hecke, M. Programmable mechanical metamaterials. *Phys. Rev. Lett.* **113**, 175503 (2014).
24. Babaee, S. et al. 3d soft metamaterials with negative poisson's ratio. *Adv. Mater.* **25**, 5044–5049 (2013).
25. Luo, C. et al. Design, manufacturing and applications of auxetic tubular structures: a review. *Thin-Walled Struct.* **163**, 107682 (2021).
26. Zhang, X. Y. et al. A novel type of tubular structure with auxeticity both in radial direction and wall thickness. *Thin-Walled Struct.* **163**, 107758 (2021).
27. Ren, X., Shen, J., Ghaedizadeh, A., Tian, H. & Xie, Y. M. Experiments and parametric studies on 3d metallic auxetic metamaterials with tuneable mechanical properties. *Smart Mater. Struct.* **24**, 095016 (2015).
28. Zhang, X. Y., Ren, X., Wang, X. Y., Zhang, Y. & Xie, Y. M. A novel combined auxetic tubular structure with enhanced tunable stiffness. *Compos. B Eng.* **226**, 109303 (2021).
29. Chen, Q. & Pugno, N. M. In-plane elastic buckling of hierarchical honeycomb materials. *Eur. J. Mech. A/Solids* **34**, 120–129 (2012).
30. Lakes, R. & Elms, K. Indentability of conventional and negative poisson's ratio foams. *J. Compos. Mater.* **27**, 1193–1202 (1993).
31. Yang, S., Chalivendra, V. B. & Kim, Y. K. Fracture and impact characterization of novel auxetic kevlar®/epoxy laminated composites. *Compos. Struct.* **168**, 120–129 (2017).
32. Lakes, R. S. & Witt, R. Making and characterizing negative poisson's ratio materials. *Int. J. Mech. Eng. Educ.* **30**, 50–58 (2002).
33. Alderson, A., Rasburn, J. & Evans, K. E. Mass transport properties of auxetic (negative poisson's ratio) foams. *Phys. Status Solidi (B)* **244**, 817–827 (2007).
34. Gatt, R. et al. Hierarchical auxetic mechanical metamaterials. *Sci. Rep.* **5**, 8395 (2015).
35. Alderson, K. et al. Auxetic warp knit textile structures. *Phys. Status Solidi (B)* **249**, 1322–1329 (2012).
36. Masters, I. & Evans, K. Models for the elastic deformation of honeycombs. *Compos. Struct.* **35**, 403–422 (1996).
37. Grima, J. N. & Evans, K. E. Auxetic behavior from rotating squares. *J. Mater. Sci. Lett.* **19**, 1563–1565 (2000).
38. Alderson, A. & Evans, K. Rotation and dilation deformation mechanisms for auxetic behaviour in the α-cristobalite tetrahedral framework structure. *Phys. Chem. Miner.* **28**, 711–718 (2001).
39. Ha, C. S., Plesha, M. E. & Lakes, R. S. Chiral three-dimensional isotropic lattices with negative poisson's ratio. *Phys. Status Solidi (B)* **253**, 1243–1251 (2016).
40. Rens, R. & Lerner, E. Rigidity and auxeticity transitions in networks with strong bond-bending interactions. *Eur. Phys. J. E* **42**, 114 (2019).
41. Milton, G. W. Composite materials with poisson's ratios close to - 1. *J. Mech. Phys. Solids* **40**, 1105–1137 (1992).
42. Lim, T.-C. A perfect 2d auxetic sliding mechanism based on an islamic geometric pattern. *Eng. Res. Express* **3**, 015025 (2021).
43. Reid, D. R., Pashine, N., Bowen, A. S., Nagel, S. R. & de Pablo, J. J. Ideal isotropic auxetic networks from random networks. *Soft Matter* **15**, 8084–8091 (2019).
44. Grima, J. N. et al. On the auxetic properties of generic rotating rigid triangles. *Proc. R. Soc. A: Math. Phys. Eng. Sci.* **468**, 810–830 (2012).
45. Grima, J. N., Zammit, V., Gatt, R., Alderson, A. & Evans, K. E. Auxetic behaviour from rotating semi-rigid units. *Phys. Status Solidi (B)* **244**, 866–882 (2007).
46. Deng, B., Yu, S., Forte, A. E., Tournat, V. & Bertoldi, K. Characterization, stability, and application of domain walls in flexible mechanical metamaterials. *Proc. Natl Acad. Sci. USA* **117**, 31002–31009 (2020).
47. Maxwell, J. C. L. On the calculation of the equilibrium and stiffness of frames. *The London, Edinburgh, and Dublin Philosophical Magazine and Journal of Science* Vol. 27, 294–299 (Taylor & Francis group, 1864).
48. Calladine, C. Buckminster Fuller's "tensegrity" structures and Clerk Maxwell's rules for the construction of stiff frames. *Int. J. Solids Struct.* **14**, 161–172 (1978).
49. Guest, S. & Hutchinson, J. On the determinacy of repetitive structures. *J. Mech. Phys. Solids* **51**, 383–391 (2003).
50. Mitschke, H., Schröder-Turk, G. E., Mecke, K., Fowler, P. W. & Guest, S. D. Symmetry detection of auxetic behaviour in 2d frameworks. *EPL (Europhys. Lett.)* **102**, 66005 (2013).
51. Grima, J. N., Mizzi, L., Azzopardi, K. M. & Gatt, R. Auxetic perforated mechanical metamaterials with randomly oriented cuts. *Adv. Mater.* **28**, 385–389 (2016).
52. Goswami, D., Liu, S., Pal, A., Silva, L. G. & Martinez, R. V. 3d-architected soft machines with topologically encoded motion. *Adv. Funct. Mater.* **29**, 1808713 (2019).
53. Mirzaali, M., Janbaz, S., Strano, M., Vergani, L. & Zadpoor, A. A. Shape-matching soft mechanical metamaterials. *Sci. Rep.* **8**, 1–7 (2018).
54. Wenz, F. et al. Designing shape morphing behavior through local programming of mechanical metamaterials. *Adv. Mater.* **33**, 2008617 (2021).
55. Mitschke, H., Robins, V., Mecke, K. & Schröder-Turk, G. E. Finite auxetic deformations of plane tessellations. *Proc. R. Soc. A Math. Phys. Eng. Sci.* **469**, 20120465 (2013).
56. Lerner, E., DeGiuli, E., Düring, G. & Wyart, M. Breakdown of continuum elasticity in amorphous solids. *Soft Matter* **10**, 5085–5092 (2014).
57. Coxeter, H. & Greitzer, S. L. *Collinearity and Concurrence*, 51-79 (Mathematical Association of America, 1967).

58. Bossart, A., Dykstra, D. M. J., van der Laan, J. & Coulais, C. Oligomodal metamaterials with multifunctional mechanics. Proceedings of the National Academy of Sciences 118 https://www.pnas.org/content/118/21/e2018610118 (2021).
59. Formlabs. Elastic Resin for Soft Flexible Parts. Rev. 1. (2019).
60. Ansys®. Ansys Mechanical, Release 19 R2 (2019).
61. Ansys®. *Ansys Mechanical APDL Theory Reference-Element Library*. Release 15.0 (2013).

Acknowledgements

G.D. acknowledges support from Fondecyt Grant No. 1210656. A.S.N. thanks Fondecyt Regular 1190324 and Financiamiento Basal para Centros Científicos y Tecnológicos de Excelencia FB 0807. D.A. acknowledges funding by the National Agency for Research and Development (ANID)/Scholarship Program/DOCTORADO NACIONAL/2019 - 21192070. This work was funded by ANID - Millenium Science Initiative Program - Code NCN17_092. We also thank C. Coulais and C. Falcon for the helpful discussions on auxetics.

Author contributions

All authors designed research, performed research, analysed data, and contributed to the manuscript preparation. G.D. and A.S.N. conceived the project. H.P. and R.S. tested and constructed the 3D printed materials. F.G. designed and performed the finite element simulations. D.A. developed the theoretical formalism and performed the numerical simulations.

Competing interests

The authors declare no competing interests.

Additional information

Supplementary information The online version contains supplementary material available at https://doi.org/10.1038/s42005-022-00876-5.

Correspondence and requests for materials should be addressed to Gustavo Düring.

Peer review information *Communications Physics* thanks Xin Ren and the other, anonymous, reviewer(s) for their contribution to the peer review of this work. Peer reviewer reports are available.

Reprints and permission information is available at http://www.nature.com/reprints

Publisher's note Springer Nature remains neutral with regard to jurisdictional claims in published maps and institutional affiliations.